



Metal Ions Induced Secondary Structure Rearrangements: Mechanically Interlocked Lasso vs Unthreaded Branched- Cyclic Topoisomers

Journal:	<i>Analyst</i>
Manuscript ID	AN-ART-01-2018-000138.R2
Article Type:	Paper
Date Submitted by the Author:	17-Apr-2018
Complete List of Authors:	Jeanne dit fouque, Kevin ; Florida International University, Chemistry and Biochemistry Moreno, Javier; Florida International University, Chemistry and Biochemistry Hegemann, Julian; University of Illinois at Urbana–Champaign, Department of Chemistry, Roger Adams Laboratory; Philipps-University Marburg, e. Department of Chemistry, Biochemistry; LOEWE Center for Synthetic Microbiology Zirah, Severine; National MUseum of Natural History Rebuffat, Sylvie; National MUseum of Natural History, Fernandez-Lima, Francisco; Florida International University, Chemistry and Biochemistry

Metal Ions Induced Secondary Structure Rearrangements: Mechanically Interlocked Lasso vs Unthreaded Branched-Cyclic Topoisomers

Kevin Jeanne Dit Fouque,[†] Javier Moreno,[†] Julian D. Hegemann,[‡] Séverine Zirah,[§] Sylvie Rebuffat,[§] and Francisco Fernandez-Lima^{*,†}

[†] Department of Chemistry and Biochemistry, Florida International University, Miami, FL 33199, USA.

[‡] Department of Chemistry, University of Illinois, Urbana-Champaign, IL 61801, USA.

[§] Laboratory Molecules of Communication and Adaptation of Microorganisms, National Museum of Natural History, Sorbonne Univ, 75005 Paris, France.

ABSTRACT: Metal ions can play a significant role in a variety of important functions in protein systems including cofactor for catalysis, protein folding, assembly, structural stability and conformational change. In the present work, we examined the influence of alkali (Na, K and Cs), alkaline earth (Mg and Ca) and transition (Co, Ni and Zn) metal ions on the conformational space and analytical separation of mechanically interlocked lasso peptides. Cyanodin I, sphingonodin I, caulonodin III and microcin J25, selected as models of lasso peptides, and their respective branched-cyclic topoisomers were submitted to native nESI trapped ion mobility spectrometry – mass spectrometry (TIMS-MS). The high mobility resolving power of TIMS permitted to group conformational families regardless of the metal ion. The lower diversity of conformational families for cyanodin I as compared to the other lasso peptides supports that cyanodin I probably forms tighter binding interactions with metal ions limiting their conformational space in the gas-phase. Conversely, the higher diversity of conformational families for the branched-cyclic topologies further supports that the metal ions probably interact with a higher number of electronegative groups arising from the fully unconstrained C-terminal part. A correlation between the lengths of the loop and the C-terminal tail with the conformational space of lasso peptides becomes apparent upon addition of metal ions. It was shown that the threaded C-terminal region in lasso peptides allows only for distinct interactions of the metal ion with either residues in the loop or tail region. This limits the size of the interacting region and apparently leads to a bias of metal ion binding in either the loop or tail region, depending whichever section is larger in the respective lasso peptide. For branched-cyclic peptides, the non-restricted C-terminal tail allows metal coordination by residues throughout this region, which can result in gas-phase structures that are sometimes even more compact than the lasso peptides. The high TIMS resolution also resulted in the separation of almost all lasso and branched-cyclic topoisomer metal ions ($r \sim 2.1$ on average). It is also shown that the metal incorporation (e.g., doubly cesiated species) can lead to the formation of a simplified IMS pattern (or preferential conformers), which results in baseline analytical separation and discrimination between lasso and branched-cyclic topologies using TIMS-MS.

Metal ions play a vital role in many biological processes.¹ They act in a variety of important functions in protein systems including enzyme catalysis, protein folding, assembly, structural stability and conformational change.^{2, 3} The presence or absence of a specific metal ion is crucial to the conformational space and/or chemical functionality of over one third of all proteins.^{1, 4} Several structural studies aimed to determine the binding site locations,^{5, 7} the nature of metal ion coordination,⁸⁻¹⁰ and the role of metal-ligand interactions on structure and function.^{11, 12} Interactions between metal ions and biomolecules have been investigated using well established techniques such as

circular dichroism,^{13, 14} nuclear magnetic resonance (NMR) spectroscopy,^{15, 16} and x-ray crystallography.^{17, 18} Furthermore, the structures of metal-containing peptides and proteins in the gas-phase have been reported using mass spectrometry¹⁹⁻²³ equipped with soft ionization sources such as electrospray ionization (ESI).²⁴ Interestingly, the addition of metal ions often influences the fragmentation patterns upon activation.²⁵⁻²⁸ In addition, the potential of metal ions to differentiate isomer species, which present the same fragmentation pattern, has been shown using tandem mass spectrometry.²⁹⁻³³ All these results suggest the existence of highly-specific metal-binding sites.

1
2
3 The interaction of peptides and proteins with metal ions
4 has been a subject of considerable interest in ion
5 mobility spectrometry coupled to mass spectrometry
6 (IMS-MS) since the pioneering work of Clemmer and
7 Jarrold.³⁴⁻⁴² These studies showed the potential of IMS-
8 MS to provide a more detailed understanding of the
9 basic interactions that occur and represent an important
10 step in the conformational engineering of peptides and
11 proteins. In addition, the implementation of the IMS
12 technique makes the use of metal ions a powerful tool
13 for the separation of isomers which are present in close
14 conformational spaces. In fact, metalated biomolecules
15 in the gas phase tend to differ in conformation from
16 their protonated analogs, as the metal ion can be
17 multiply charged, can bind to single/multiple sites,
18 and/or coordinates differently because of specific
19 chemistry.⁴³ If these deviations are unequal for two
20 isomer species, metalation can potentially enhance their
21 separation in IMS devices with modest resolving power
22 ($R \sim 30-60$).⁴⁴⁻⁴⁷ The push for higher resolution and
23 sensitivity has led to the development of other forms of
24 IMS devices, including trapped IMS (TIMS).^{48, 49} The
25 coupling of TIMS-MS⁴⁸⁻⁵³ has found multiple
26 applications in analytical workflows which need high
27 mobility resolving power (R up to ~ 400).⁵⁴ TIMS-MS
28 devices have proven useful for rapid separation and
29 structural elucidation of biomolecules,^{53, 55-65} for
30 screening⁵⁵ and targeted^{51, 53} analysis of complex
31 mixtures, tracking isomerization kinetics,⁵⁶⁻⁵⁸
32 characterizing the conformational spaces of peptides,⁶⁶
33 separation of D-amino acid containing peptides,⁶⁷
34 DNA,⁵⁹ proteins,^{68, 69} and macromolecular complexes in
35 native and denatured states.⁷⁰ The effect of metal
36 incorporation in peptide systems has not been reported
37 using TIMS devices, although similar analytical
38 enhancement to those observed previously with other
39 variants of IMS are expected.

40 Research on metal-peptide systems provides a basis for
41 understanding metal interactions occurring in
42 biochemically relevant systems. In particular, class II
43 lasso peptides are a structurally fascinating class of
44 ribosomally synthesized and post-translationally
45 modified peptides (RiPPs) exhibiting a unique
46 mechanically interlocked topology.^{71, 72} They display a
47 rigid and compact structure where the C-terminal tail is
48 threaded through and trapped within an N-terminal
49 macrolactam ring, leading to a [1]rotaxane type structure
50 (Figure S1). Strong sterical constraints, which come from
51 bulky amino acids located above and below the
52 macrolactam ring that are called plugs, stabilize the
53 entropically disfavored lasso structure. Many lasso
54 peptides were discovered through genome mining
55 approaches and isolation and characterization of new
56 representatives of this RiPP family is still an active area

of research.⁷³⁻⁷⁸ Diverse biological activities have been
reported for class II lasso peptides, including
antimicrobial, enzyme inhibitory or receptor
antagonistic properties.^{71, 72} The extraordinary rigid and
compact structure of the mechanically interlocked lasso
topologies, together with their panel of biological
activities makes them a promising scaffold for next
generation drug design.^{79, 80} One limitation to the
activity and further developments of lasso peptides is
the unthreading of the C-terminal tail, a trend reported
for certain lasso peptides, which yield their
corresponding branched-cyclic topoisomers, although
there are also numerous examples of lasso peptides that
are resistant to thermally-induced unthreading.^{73, 81-83}

In this study, four mechanically interlocked lasso
peptides, caulonodin III, microcin J25, sphingonodin I
and syanodin I, with their corresponding unthreaded
branched-cyclic topoisomers were investigated using
native nESI-TIMS-MS (Table 1). These four lasso
peptides were specifically selected according to the
lengths of the loop and the C-terminal tail region which
could provide different binding interactions with the
metal ions. In the following discussion, a special
emphasis will be placed on the influence of alkali (Na, K
and Cs), alkaline earth (Mg and Ca) and transition (Co,
Ni and Zn) metal ions on lasso and branched-cyclic
topoisomer ion conformation and separation.

EXPERIMENTAL SECTION

Materials and Reagents

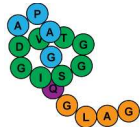

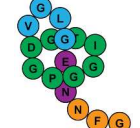


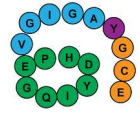
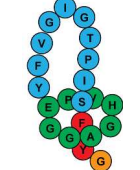

Microcin J25 was produced, as described previously,⁸⁴ by
cultivation of *Escherichia coli* MC4100 harboring the
plasmid pTUC202,⁸⁵ in M63 medium at 37 °C for 16 h.
Caulonodin III,⁷³ sphingonodin I,⁷³ and syanodin I,⁷³
were produced heterologously in *E. coli* BL21 (DE3), as
described elsewhere (Table S1). Briefly, the purification
procedures were started with centrifugation to separate
cell pellets and culture supernatants. Microcin J25 was
extracted from the culture supernatants by solid phase
extraction using SepPak C₈ or C₁₈ reversed-phase
cartridges (Waters). The elution was performed using
water with 0.1 % formic acid and acetonitrile mixtures
with increasing content of acetonitrile, and the fractions
of interest were then evaporated under reduced
pressure. A second purification step was performed by
reversed-phase high performance liquid
chromatography (HPLC). Caulonodin III, sphingonodin
I and syanodin I were isolated from cell pellets by
extraction with methanol. The resulting extracts were
directly subjected to HPLC purification steps as
described previously.

The branched-cyclic peptide of syanodin I was obtained
by heating the lasso peptide at 95°C for 3 h and was

1
2
3
4
5
6
7
8
9
10
11
12
13
14
15
16
17
18
19
20
21
22
23
24
25
26
27
28
29
30
31
32
33
34
35
36
37
38
39
40
41
42
43
44
45
46
47
48
49
50
51
52
53
54
55
56
57
58
59
60

subsequently purified by reversed-phase HPLC. For caulonodin III, microcin J25 and sphingonodin I, which

Table 1. Summary of the studied lasso and branched-cyclic peptides. The macrolactam rings are highlighted in green, the loops in blue, the plugs in red and the C-terminal tails in orange. The proposed plugs-of lasso peptides, for which the 3D structures have not been determined, are colored in purple.

Peptide	Sequence	Molecular mass (Da)	Topology
Syanodin I	GISGGTVD ₈ APAGQGLAG ₁₆	1409.50	
Syanodin I branched-cyclic	GISGGTVD ₈ APAGQGLAG ₁₆	1409.50	
Sphingonodin I	GPGGITGD ₈ VGLGENNFG ₁₇	1542.61	
Sphingonodin I branched-cyclic	GPGGITGD ₈ VGLGENNFG ₁₇	1542.61	
Caulonodin III	GQIYDHPE ₈ VGIGAYGCE ₁₇	1789.92	
Caulonodin III branched-cyclic	GQIYDHPE ₈ VGIGAYGCE ₁₇	1789.92	
Microcin J25	GGAGHVPE ₈ YFVGIGTPISFYG ₂₁	2107.32	
Microcin J25 branched-cyclic	GGAGHVPE ₈ YFVGIGTPISFYG ₂₁	2107.32	

are heat stable lasso peptides, topoisomeric variants were obtained by solid-phase synthesis from Genepep (St Jean de Védas, France). The carbonate salts of Na, K, Cs, Mg, Ca, Co, Ni and Zn were purchased from Acros Organics (New Jersey, USA). The peptides were dissolved in 10 mM NH₄Ac (native conditions) to 5 μM with or without 70 μM of a carbonate salt. The instrument was initially calibrated using the Tuning Mix³⁰ from Agilent (Santa Clara, CA).

TIMS-MS Experiments

We employed a custom nESI-TIMS unit coupled to an Impact Q-TOF mass spectrometer (Bruker, Billerica, MA).^{48, 49} The TIMS unit is run by custom software in LabView (National Instruments) synchronized with the MS platform controls.⁴⁹ Sample aliquots (10 μL) were loaded in a pulled-tip capillary biased at 700-1200 V to the MS inlet. TIMS separation depends on the gas flow velocity (v_g), elution voltage ($V_{elution}$), ramp time (t_{ramp}) and base voltage (V_{out}).^{48, 86} The mobility, K , is defined by:

$$K = \frac{v_g}{E} \cong \frac{A}{(V_{elution} - V_{out})} \quad (1)$$

The mobility calibration was determined using known reduced mobilities of Tuning Mix components (K_0 of 1.013, 0.835, and 0.740 cm²/(V.s) for respective m/z 622, 922, and 1222) using the method previously described.⁵⁰ The buffer gas was N₂ at ambient temperature (T) with v_g set by the pressure difference between the funnel entrance ($P_1 = 2.6$ mbar) and exit ($P_2 = 1.1$ mbar, Figure S2). An rf voltage of 200 V_{pp} at 880 kHz was applied to all electrodes. A typical scan rate ($Sr = \Delta V_{ramp}/t_{ramp}$) of 0.56 V/ms was used. The measured mobilities were converted into CCS (Å²) using the Mason-Schamp equation:

$$\Omega = \frac{(18\pi)^{1/2}}{16} \frac{q}{(k_B T)^{1/2}} \left(\frac{1}{m} + \frac{1}{M}\right)^{1/2} \frac{1}{N} \times \frac{1}{K} \quad (2)$$

where q is the ion charge, k_B is the Boltzmann constant, N is the gas number density, m is the ion mass, and M is the gas molecule mass.⁸⁶ The IMS peaks were fitted with Gaussian distributions using *OriginPro 2016*. The resolution r is defined as $r = 1.18^*(\Omega_2 - \Omega_1)/(w_1 + w_2)$, where w is the full peak width at half maximum (FWHM).

RESULTS AND DISCUSSION

Influence of Metal Ions on Lasso and Branched-Cyclic Topoisomer Ion Conformation

The distribution of lasso and branched-cyclic peptide ions (either protonated, or containing metal ions) mostly displayed [M+2H]²⁺, [M+H+X]²⁺ and/or [M+2X]²⁺ charge state species when using native nESI. Typical high resolution TIMS spectra for protonated and metalated forms of the individual lasso peptides (caulonodin III, microcin J25, sphingonodin I and syanodin I) and their corresponding unthreaded branched-cyclic topoisomers are shown in Figures 1 and S3 and their collision cross sections (CCS) are listed in Table S2-S5. As previously reported,⁸⁷ the high resolution of TIMS permitted the separation of multiple IMS bands for the protonated lasso and branched-cyclic peptides (highlighted in black in Figure 1). The observation of multiple compact and extended conformations suggested the presence of several combinations of intramolecular charge-driven and/or hydrogen bond interactions, especially between residues in the flexible C-terminal tail (highlighted in orange in Table 1) and the macrolactam ring (in green).⁸⁸⁻⁹⁰ It is difficult to predict the charge localization as well as the effect of substituting protons for metal ions on the conformational space. In fact, a previous work has shown that replacing a proton by a sodium in polyaniline chains reduces the abundance of globular structures by promoting more extended conformations,⁹¹ while another study reported a decrease in CCS leading to more compact structures.³⁷

These results provide evidence that sodium ions interact in different ways with functional groups of the peptide backbone and thereby are stabilizing the gas-phase conformation. We predict that the multiple interactions between the metal ions and the peptides under a given conformation will probably be stabilized through the electronegative groups.

Although solution conditions were designed to favor metalated peptide ions, protonated species were also observed. All of the metalated species studied here led to noticeable changes in the CCS distributions as compared to the protonated species (Figures 1 and S3). CCS values generally increased upon incorporating metal ions for lasso peptides except for syanodin I. For example, the doubly cesiated species (highlighted in dark orange in Figure 1a) of sphingonodin I, caulonodin III and microcin J25 led to a relative mobility increase of 4.0%, 3.2% and 6.5%, respectively. Conversely, the relative CCS appears to be smaller when replacing a proton by metal ions in syanodin I (Figures 1 and S3). For example, the doubly cesiated species (highlighted in dark orange in Figure 1a) led to a relative mobility decrease of 1.5%. This suggests that syanodin I probably forms tighter binding interactions with these metals than sphingonodin I, caulonodin III and microcin J25. In the case of the branched-cyclic peptides, the shifts of the metalated compared to protonated species are generally less pronounced than for the lasso peptides (Figure 1). This suggests that the metal ions probably bind with a higher number of electronegative groups than the lasso peptides. In fact, metal ions can more easily interact with the full flexible C-terminal part of the unconstrained branched-cyclic peptides than the mechanically interlocked topology (Figure 1).

Comparison of the TIMS profiles of the metalated species showed common bands regardless of the metal ion incorporated (Figures 1d, 1e and S3 and Tables S2-S5). For example, IMS profiles for syanodin I can be grouped in at least four conformational families (Figures 1d and S3 and Table S2). The IMS band at ~377 Å² is observed by adding one or two sodium, a magnesium and a calcium. The IMS band at ~387 Å² is observed in the protonated, cesiated, doubly sodiated, magnesiated and calciated species. The IMS band at ~394 Å² is common to all the metal ions except with two sodium and a calcium. The motif at ~401 Å² is preserved for the protonated, singly alkali and alkaline earth metalated ions.

In the case of sphingonodin I, the IMS profiles can be grouped in at least six conformational families (Figures 1d and S3 and Table S3). The IMS band at ~396 Å² is observed with the protonated, calciated and nickelated species. The IMS band at ~401 Å² is observed with the protonated species and by adding two sodium, a

1
2
3 magnesium, a calcium and a zinc. The IMS band at ~ 404
4 \AA^2 is observed for the protonated and all the metalated
5 species except for the doubly sodiated and cesiated
6 species. The IMS band at ~ 410 \AA^2 is observed for the
7 transition metal ions, magnesium and all the alkali
8 metal ions except in the case of the doubly cesiated
9 species. The IMS band at ~ 415 \AA^2 is common to all the
10 investigated metal ions, while the IMS band at ~ 420 \AA^2
11 is observed for all singly alkali and doubly sodiated
12 species.

13 In the case of caulonodin III, the IMS profiles can be
14 grouped in at least five conformational families (Figure
15 1d and S3 and Table S4). The IMS band at ~ 436 \AA^2 is
16 observed with the alkaline earth and zincated species.
17 The IMS band at ~ 440 \AA^2 is observed with the
18 protonated species and by adding alkaline earth and
19 transition metal ions. The IMS band at ~ 446 \AA^2 is
20 common to all the metal ions except for the cesiated
21 species. The IMS band at ~ 449 \AA^2 is preserved for one
22 cesium, two potassium and for all alkaline earth and
23 transition metal ions. The IMS band at ~ 454 \AA^2 is
24 observed only for the doubly cesiated, cobaltiated and
25 zincated species.

26 In the case of microcin J25, the IMS profiles can be
27 grouped in at least six conformational families (Figures
28 1d and S3 and Table S5). The IMS band at ~ 476 \AA^2 is
29 observed with the protonated, singly sodiated and
30 potassiumated and magnesiated species. The IMS band at
31 ~ 482 \AA^2 is observed with the protonated species and by
32 adding one sodium, a magnesium, a cobalt and a nickel.
33 The IMS band at ~ 490 \AA^2 is observed for the protonated
34 and all the metalated species except for the doubly alkali
35 and singly cesiated species. The IMS band at ~ 496 \AA^2 is
36 observed for the protonated, doubly sodiated and
37 potassiumated and all the alkaline earth and transition
38 metalated ions. The IMS band at ~ 505 \AA^2 is common to
39 all the investigated metal ions except for the sodiated
40 and singly potassiumated species. The IMS band at ~ 510 \AA^2
41 is observed for the protonated, singly cesiated, doubly
42 potassiumated and all the transitions metalated species.

43 In the case of the branched-cyclic form of cyanodin I, at
44 least nine conformational families are observed for all
45 the investigated metal ions (Figures 1e and S3 and Table
46 S2). The IMS band at ~ 379 \AA^2 is observed with the
47 calciated, cobaltiated and zincated species. The IMS
48 band at ~ 385 \AA^2 is observed with the protonated species
49 and by adding one potassium, one cesium and all the
50 alkaline earth and transition metal ions. The IMS band
51 at ~ 390 \AA^2 is observed for the protonated, doubly
52 potassiumated, alkaline earth and transition metalated
53 species. The IMS band at ~ 394 \AA^2 is observed for the
54 protonated and by incorporating one potassium, a
55 magnesium, a nickel and a zinc metal ion. The IMS band
56 at ~ 397 \AA^2 is common to all the investigated metal ions

except for the singly cesiated, doubly sodiated and
nickelated species. The IMS band at ~ 401 \AA^2 is observed
for all the metal ions except for the doubly sodiated and
cesiated and alkaline earth metalated species. The IMS
band at ~ 405 \AA^2 is observed for all the metal ions except
for the protonated, potassiumated, singly cesiated and
magnesiated species. The IMS band at ~ 409 \AA^2 is
common to all the studied metal ions except for the
protonated and the singly sodiated and cesiated species.
The IMS band at ~ 417 \AA^2 is only observed by adding two
potassium.

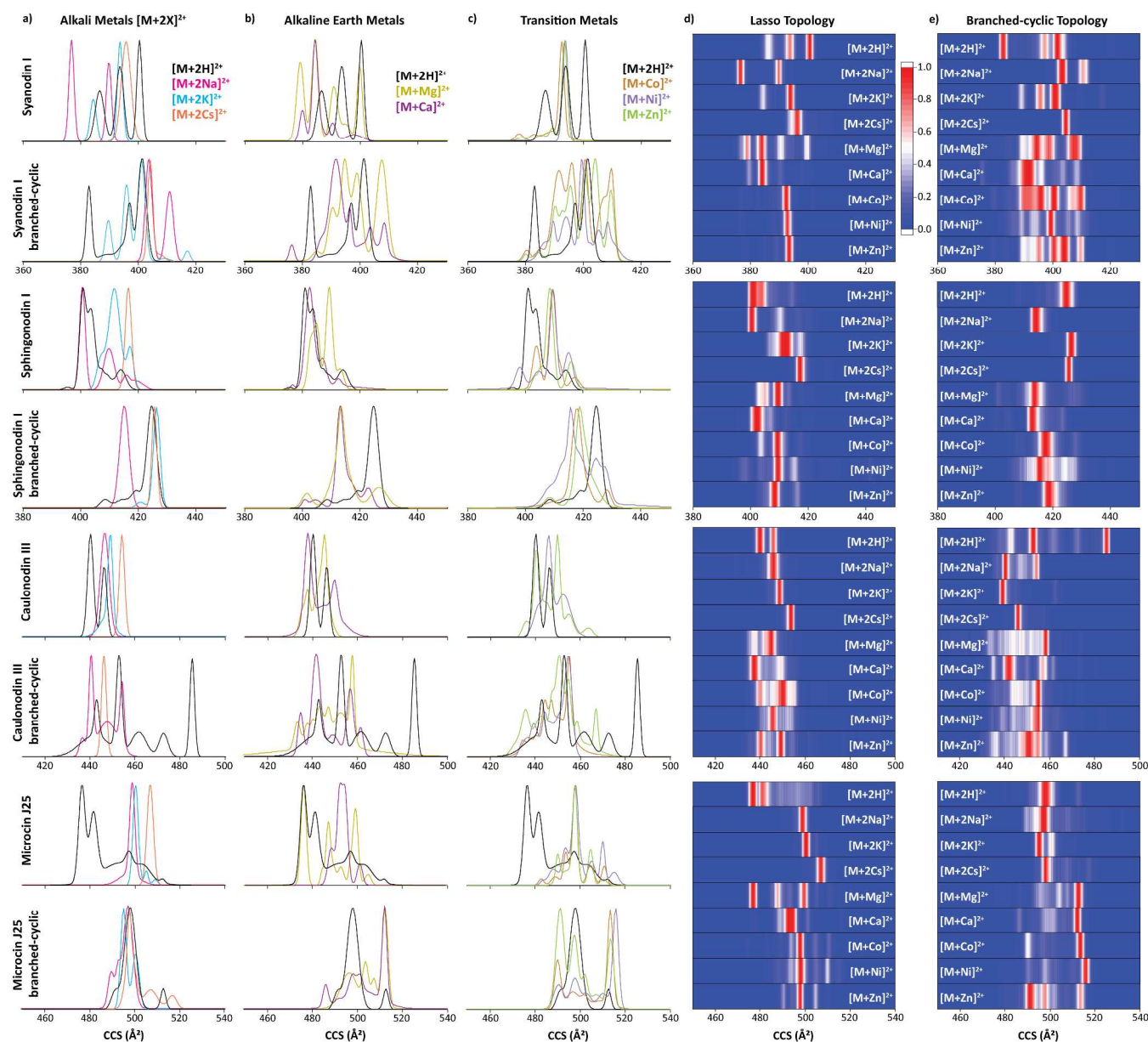
In the case of the branched-cyclic form of sphingonodin
I, the IMS profiles of all the metal ions studied can be
divided in at least six conformational families (Figures 1e
and S3 and Table S3). The IMS band at ~ 404 \AA^2 is
observed by incorporating one sodium, a magnesium
and a calcium metal ion. The IMS band at ~ 408 \AA^2 is
observed for the protonated, singly potassiumated and all
the transition metalated species. The IMS band at ~ 415
 \AA^2 is observed with the protonated species and by
adding two sodium, a magnesium, a calcium and a
nickel metal ion. The IMS band at ~ 419 \AA^2 is common to
the protonated, singly sodiated, doubly potassiumated and
all the transition metalated species. The IMS band at
 ~ 425 \AA^2 is observed for all the metal ions except for the
sodiated, magnesiated, cobaltiated and zincated species.
The IMS band at ~ 429 \AA^2 is common for the singly
alkali, magnesiated, cobaltiated and nickelated species.

In the case of caulonodin III branched-cyclic, the IMS
profiles can be grouped in at least nine conformational
families (Figures 1e and S3 and Table S4). The IMS band
at ~ 433 \AA^2 is only observed by incorporating a sodium
metal ion. The IMS band at ~ 438 \AA^2 is observed for all
the metal ions except for the singly potassiumated and
cesiated species. The IMS band at ~ 443 \AA^2 is common to
all the studied metalated species. The IMS band at ~ 448
 \AA^2 is observed by adding one cesium, two sodium, a
magnesium, a calcium, a cobalt and a zinc metal ion.
The IMS band at ~ 454 \AA^2 is observed for all metal ions
except for the cesiated and doubly potassiumated species.
The IMS band at ~ 460 \AA^2 is observed for all the metal
ions except for the doubly sodiated and cesiated,
cobaltiated and nickelated species. The IMS band at
 ~ 472 \AA^2 is observed for the protonated, singly
potassiumated and cesiated and zincated species. The IMS
bands at ~ 480 and ~ 485 \AA^2 are characteristic of the
insertion of one potassium and without metal ion,
respectively.

In the case of the branched-cyclic form of microcin J25,
the IMS profiles of all the metal ions studied can be
divided in at least seven conformational families
(Figures 1e and S3 and Table S5). The IMS band at ~ 477
 \AA^2 is observed by incorporating a single sodium,
potassium and cesium metal ion. The IMS band at ~ 487

\AA^2 is observed only for the sodiated and calcated species. The IMS band at $\sim 491 \text{\AA}^2$ is observed with all the metal ions except for the singly sodiated, doubly cesiated and magnesiated species. The IMS band at $\sim 498 \text{\AA}^2$ is common to all the investigated metalated species. The IMS band at $\sim 505 \text{\AA}^2$ is observed for the singly sodiated and potassiumated, doubly cesiated, magnesiated and all the transition metalated species. The IMS band at $\sim 513 \text{\AA}^2$ is common in the protonated species and by incorporating all the alkaline earth and transition metal ions. The conformation at $\sim 517 \text{\AA}^2$ is only observed by adding two cesium and a nickel metal ion.

The lower number of conformational families for cyanodin I as compared to the other lasso peptides suggests that cyanodin I forms tighter binding interactions with all the studied metal ions limiting their conformational changes in the gas-phase. Conversely, the higher number of conformational families for the branched-cyclic topologies further supports that the metal ions probably interact with a higher number of electronegative groups arising from the unconstrained C-terminal part as compared to the mechanically interlocked lasso structures.



1
2
3 **Figure 1.** Typical TIMS spectra of lasso and branched-cyclic topoisomers of the protonated (black), sodiated (magenta),
4 potassiated (light blue), cesiated (dark orange), magnesiated (yellow), calciated (purple), cobaltiated (brown), nickelated (light
5 purple) and zincated (light green) species. Corresponding heat maps are shown in d) and e). A typical Sr of 0.56 V/ms was used.

6 Comparison of CCS for species with similar masses
7 provides some insight about the conformational range
8 of different isomeric structures that are present in the
9 gas-phase. For lasso peptides, due to larger structural
10 constraints in their secondary structure, it is expected
11 that the interaction with the metal ion will have a lower
12 effect than for the branched-cyclic peptides. That is,
13 secondary structure elements of the mechanically
14 interlocked lasso topologies may be preserved or
15 stabilized upon metal ion binding while more changes
16 are expected for the branched-cyclic topologies due to
17 the unthreaded flexible C-terminal part. The relatively
18 complex TIMS distribution (i.e., existence of multiple
19 bands) makes it challenging to estimate the influence of
20 metalated species on the conformational spaces of the
21 lasso and branched-cyclic topologies. Therefore,
22 determination of the weighted average CCS ($\Sigma (CCS \times$
23 $Intensity) / (\Sigma Intensity)$), based on the CCS reported in
24 Table S2-S5) in order to get a unique CCS value for every
25 doubly charged species proved to be a better approach.
26 At first, we plotted the CCS values as a function of the
27 molecular mass for all the investigated species as a way
28 to assess the conformational trend (Figure 2a). A strong
29 correlation of increasing CCS with the molecular mass
30 was obtained for syanodin I, sphingonodin I, caulonodin
31 III and microcin J25 with their corresponding branched-
32 cyclic topoisomers (Figure 2a). In addition, the two
33 correlations shown in Figure S4a revealed that the
34 branched-cyclic structures are more extended than the
35 lasso ones regardless of the molecular mass.

36 Comparison between the \overline{CCS}_H and the \overline{CCS}_{Metal} enables
37 to efficiently illustrate the metalation effect on the
38 conformational spaces of the lasso and branched-cyclic
39 topoisomers (Figure 2b). The lasso structures tend to
40 expand with the metal ion adduction, as in the case of
41 sphingonodin I, caulonodin III and microcin J25.
42 However, this trend is not observed in the case of
43 syanodin I where the \overline{CCS}_{Metal} are smaller relative to the
44 \overline{CCS}_H , suggesting a compacting behavior upon
45 metalation (Figure 2b). Moreover, \overline{CCS}_{Metal} generally
46 tend to increase with the ionic radius of the metal ion
47 for the lasso peptides (Figure 2b). This trend was clearly
48 observed for the doubly alkali metalated species, for
49 which the $\overline{CCS}_{2Cs} > \overline{CCS}_{2K} > \overline{CCS}_{2Na} > \overline{CCS}_{2H}$ induced an
50 expanding of the lasso structures upon metalation. In
51 addition, this trend was also observed in the case of
52 syanodin I, for which the metalation results in a
53 compacting behavior. However, this trend was not
54 observed for all the branched-cyclic structures, involving
55 that these peptides can fully interact with metal ions

thanks to their completely flexible C-terminal part
resulting in distinct rearrangements (Figure 2b). The
nature of the metal ions showed that the divalent
metalated species generally favor the compacting or
expanding behavior for lasso peptides as compared to
the singly monovalent metalated species with similar
ionic radius (Figure 2b). These trends were clearly
observed for syanodin I and microcin J25 where the
divalent metal ions induced more compact and
extended conformations, respectively. The same trends
were also observed for the branched-cyclic peptides. The
divalent metal ions interact with a higher number of
ionic chemical bonds as compared to the singly
monovalent metal ions with the same ionic radius.

Further inspection of the lasso structures reveals that
these observations are related to the lengths of the loop
and the C-terminal tail of the lasso peptides (Figures 2c
and S4b). In fact, the steric stabilization of the C-
terminal region inside of the macrolactam ring in lasso
peptides allows only for distinct interactions of the
metal ion with either residues in the loop or tail region.
This limits the size of the interacting region and
apparently leads to a bias of metal ion binding in either
the loop or tail region,

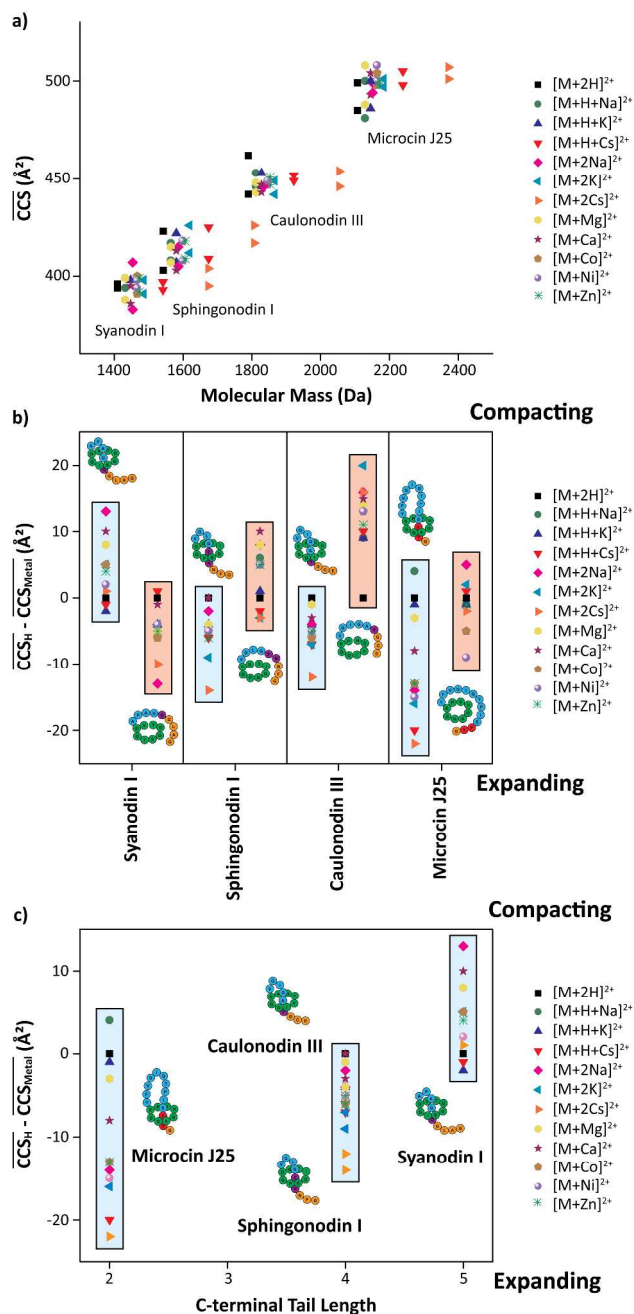


Figure 2. (a) \overline{CCS} for all lasso and branched-cyclic peptides as a function of the molecular mass of the observed protonated (black), sodiated (dark green and magenta), potassiated (dark and light blue), cesiated (red and dark orange), magnesiated (yellow), calciated (purple), cobaltiatiated (brown), nickeliated (light purple) and zincated (light green) species. (b) Effect of the metalated species on the lasso (blue) and branched-cyclic (red) conformational spaces. (c) Effect of the metalated species on the lasso conformational spaces as a function of the C-terminal length.

depending whichever section is larger in the respective lasso peptide. For example, the short loop (4 residues) and the long C-terminal tail (5 residues) of syanodin I suggest that the metal ions are interacting with the C-terminal tail, inducing a compacting of the flexible C-terminal tail (Figures 2c and S4b). Conversely, for microcin J25, the larger loop (11 residues) and the shorter C-terminal tail (2 residues) indicate that the metal ions are probably interacting with the loop, implying an expansion of this region (Figures 2c and S4b). For the unthreaded branched-cyclic peptides, incorporating a metal ion induces different type of structures by interacting in a different way with the metal ions. In fact, the branched-cyclic form of syanodin I and microcin J25 tended to expand with the metal ion adduction, while sphingonodin I and caulonodin III adopted a more compact structure. The latter behavior probably arises from the non-restricted flexible C-terminal tail that can form additional intramolecular binding interactions with the metal ions. In fact, the non-restricted C-terminal tail of the branched-cyclic topology allows metal coordination by residues throughout this region, which can result in gas-phase structures that are sometimes even more compact than the lasso peptides, for which the topology may be preserved or stabilized upon metal ion binding limiting their conformational changes.

Previous reports hypothesized that lasso peptides produced by gene clusters in proximity of a lasso peptide isopeptidase encoding gene might act like metallophores.^{92, 93} That is, that they would act as scavenger molecules for certain metal ions, which would in turn be released upon lasso peptide isopeptidase-mediated degradation inside the cells. If this hypothesis would hold true for the tested lasso peptide caulonodin III, sphingonodin I and syanodin I (microcin J25 is not produced by gene clusters with a lasso peptide isopeptidase encoding gene), a single distinct conformation would appear in the IMS distribution due to the specific interactions typical for metallophore-metal ion complexes. This was not observed with any of the tested metal ions including the typical metallophore targets as copper and iron metal ions, except for the single alkali (Na, K and Cs) species of caulonodin III and the nickeliated species of syanodin I (Figures 1, S3 and S5). In fact, multiple IMS bands with distinct CCS were observed in all these cases suggesting multiple interactions of the metal ions with the lasso peptides under these conditions.

Influence of Metal Ions on Lasso and Branched-Cyclic Topoisomer Analytical Screening

Although lasso peptides and their corresponding branched-cyclic topoisomers share the same amino acid sequence, they can be differentiated based on their

secondary structures.⁹⁴ In a previous work, we showed the potential of native nESI-TIMS-MS as a high throughput screening tool for identification of lasso and branched-cyclic topologies.⁸⁷ Briefly, TIMS-MS using fast scan rates resulted in baseline separation for doubly protonated species of sphingonodin I ($r = 2.8$, Figure S6a), caulonodin III ($r = 2.5$, Figure S7a) and microcin J25 ($r = 1.9$, Figure S8a).⁸⁷ However, only partial separation was observed for syanodin I topoisomers ($r = 0.7$, Figure 3a) using fast scan rates. A known alternative to increase the analytical power of IMS techniques is the use of metalation.⁴⁴⁻⁴⁷ In fact, metalated species tend to differ in conformation from their protonated analogs as the metal ions may bind to different sites and/or coordinate differently because of their chemical differences, potentially leading to effective IMS separation.⁴³

The effect of alkali (Na, K and Cs), alkaline earth (Mg and Ca) and transition (Co, Ni and Zn) metal ions on the TIMS separation of lasso and branched-cyclic topoisomers is illustrated in Figures 3, S6, S7 and S8 for syanodin I, sphingonodin I, caulonodin III and microcin J25, respectively. Inspection of Figure 3 shows that for all cases, except the singly sodiated ($r = 0.2$, Figure 3b) and potassiated ($r = 0.5$, Figure 3c) species, the metalated species resulted in higher IMS resolution (r , by at least a factor of 2) between the lasso and branched-cyclic topoisomers compared to the IMS resolution achieved using the protonated species, enabling their identification at fast scan rates (Table S2). Concerning sphingonodin I (Figure S6 and Table S3), caulonodin III (Figure S7 and Table S4) and microcin J25 (Figure S8 and Table S5), for which protonated species are well resolved, the metalated species generally did not improve or resulted in comparable IMS resolution as compared to the protonated species. However, several metal ions allowed to obtain higher IMS resolution in the case of the singly potassiated ($r = 4.7$, Figure S6c) and cesiated ($r = 4.8$, Figure S6d) species for sphingonodin I, the magnesiated ($r = 3.3$, Figure S7h) species for caulonodin III and the magnesiated ($r = 2.6$, Figure S8h), calciated ($r = 3.8$, Figure S8i), cobaltiased ($r = 3.2$, Figure S8j), nickeliated ($r = 3.4$, Figure S8k) and zincated ($r = 3.4$, Figure S8l) species for microcin J25. The most pronounced difference was observed for the $[M+2Na]^{2+}$ ($r = 3.4$, Figure 3e), $[M+H+Cs]^{2+}$ ($r = 4.8$, Figure S6d), $[M+Mg]^{2+}$ ($r = 3.3$, Figure S7h) and $[M+Ca]^{2+}$ ($r = 3.8$, Figure S8i) species of syanodin I, sphingonodin I, caulonodin III and microcin J25, respectively.

All these results did not display a general trend in term of IMS resolution and therefore suggest that metal ion binding rearrange lasso and branched-cyclic structures in different ways, which involves trying diverse metal ions to maximize resolution. However, a different

number of IMS bands are observed as a function of the metal ion size for the same charge state in both topoisomers. For example, while the TIMS distribution of the metalated lasso and branched-cyclic peptide ions typically consisted of multiple bands, the TIMS distribution of the doubly cesiated species resulted in a single band for each lasso and branched-cyclic peptide couple (except for microcin J25 branched-cyclic that presents two minor IMS bands),

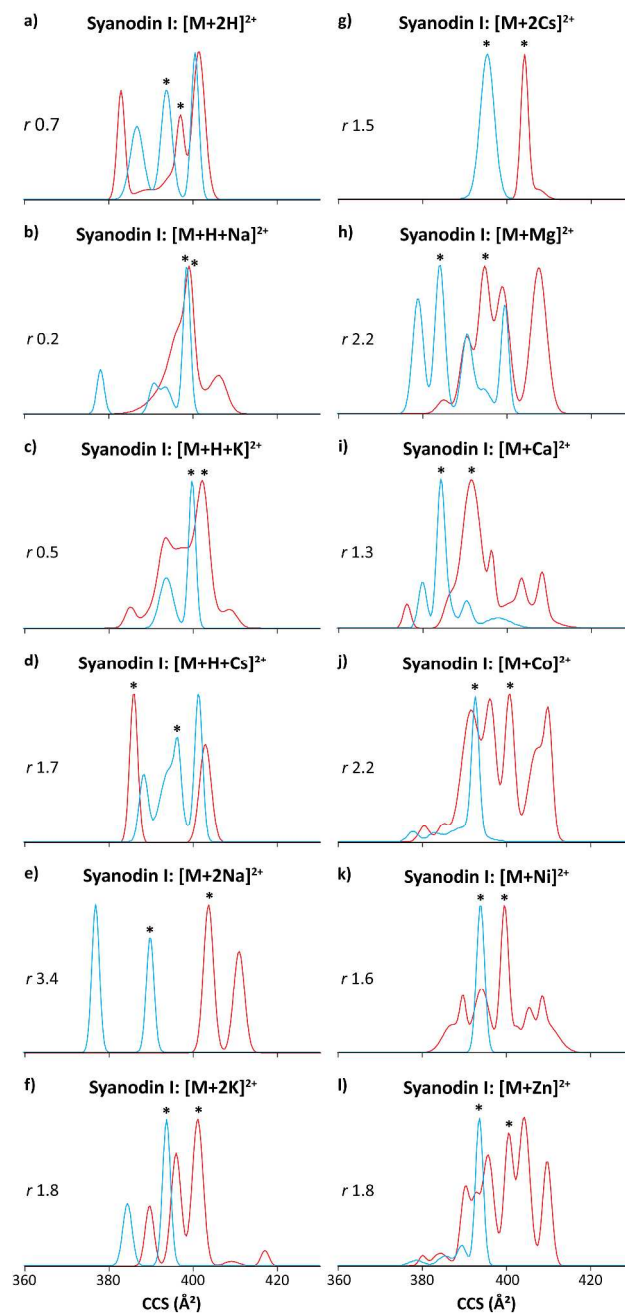


Figure 3. Typical TIMS spectra for syanodin I (blue traces) and its branched-cyclic topoisomer (red traces) in the (a)

1
2
3 protonated, (b, e) sodiated, (c, f) potassiated, (d, g)
4 cesiated, (h) magnesiated, (i) calciated, (j) cobaltiated, (k)
5 nickelated and (l) zincated form. A typical Sr of 0.56 V/ms
6 was used and the resolution (r) values are given. The peaks
7 highlighted by * symbols were taken to calculate the
8 resolution.

9 therefore improving the discrimination between these
10 topoisomers in the gas-phase (Figures 3g, S6g, S7g and
11 S8g). The presence of the two additional minor IMS
12 bands for the branched-cyclic form of microcin J25
13 (Figure S8g) could be explained by the longer length of
14 its C-terminal region (13 residues, Table 1), as compared
15 to the other branched-cyclic peptides (9 residues, Table
16 1), which significantly increase the flexibility of this
17 region, permitting additional interactions with the
18 cesium ions. These results illustrate the potential of the
19 doubly cesiated species to provide a unique
20 conformation as an efficient analytical feature for the
21 identification of the lasso fold and corresponding
22 branched-cyclic topoisomers at physiological conditions,
23 using high resolution native nESI-TIMS.

24 CONCLUSIONS

25
26 The potential of native nESI-TIMS-MS as a powerful tool
27 for the investigation of the conformational changes
28 upon alkali (Na, K and Cs), alkaline earth (Mg and Ca)
29 and transition (Co, Ni and Zn) metalation of four lasso
30 peptides (cyanodin I, sphingonodin I, caulonodin III and
31 microcin J25) and their branched-cyclic topoisomers was
32 studied. The present results showed that the nature of
33 the metal ions plays a significant role in the
34 conformational motifs, as reflected by the substantial
35 changes in the IMS distributions as compared to the
36 protonated species. In addition, the high mobility
37 resolving power of TIMS permitted to group
38 conformational families that are preserved regardless
39 of which metal ion is incorporated. The lower diversity of
40 conformational families for cyanodin I as compared to
41 the other lasso peptides supported cyanodin I probably
42 forms tighter binding interactions with metal ions
43 limiting their conformational changes in the gas-phase.
44 Conversely, the higher diversity of conformational
45 families for the branched-cyclic topologies further
46 supported that the metal ions probably interact with a
47 higher number of electronegative groups arising from
48 the fully unconstrained C-terminal part.

49 A correlation between the lengths of the loop and the C-
50 terminal tail with the conformational spaces of the lasso
51 peptides becomes apparent upon addition of metal ions.
52 The steric stabilization of the C-terminal region inside of
53 the macrolactam ring in lasso peptides allows only for
54 distinct interactions of the metal ion with either
55 residues in the loop or tail region. This limits the size of
56 the interacting region and apparently leads to a bias of

metal ion binding in either the loop or tail region,
depending whichever section is larger in the respective
lasso peptide. For branched-cyclic peptides, the non-
restricted C-terminal tail allows metal coordination by
residues throughout this region, which can result in gas-
phase structures that are sometimes even more compact
than the lasso peptides.

The high mobility resolving power of TIMS resulted in
the separation of metalated lasso and branched-cyclic
peptide ions ($r \sim 2.1$ on average). The added analytical
advantages of metalation to the nESI-TIMS-MS were
particularly illustrated in the case of cyanodin I
topoisomers, where the differences in the IMS profiles
are significantly increased with metalation. Conversely,
for the well resolved sphingonodin I, caulonodin III and
microcin J25, the metalation generally did not improve
separation and resulted in comparable IMS resolution as
found for the protonated species. Results showed that
the metal ion binding can rearrange lasso and branched-
cyclic structures in distinct ways. Moreover, metalation
(e.g., using the doubly cesiated species) can result in
simplification of the mobility profiles down to a single
conformation and thus can be utilized as a way to
maximize the analytical power of high resolution TIMS
for the discrimination of lasso and branched-cyclic
topologies at physiological conditions.

ASSOCIATED CONTENT

Supporting Information

3D representation of class II lasso peptides, scheme of the
TIMS cell, correlation of the \overline{CCS} of the doubly protonated
species of lasso and branched-cyclic peptides as a function
of the molecular mass, effect of the metalated species on
the lasso conformational spaces as a function of the loop
size, TIMS spectra of the investigated lasso peptides and
their branched-cyclic topoisomers cationized by alkali,
alkaline earth and transition metalated species, conditions
for the production of lasso peptides, and Tables of the
measured CCS and resolution for all lasso and branched-
cyclic ions. This material is available free of charge via the
Internet at <http://pubs.acs.org>.

AUTHOR INFORMATION

Corresponding Author

fernandf@fiu.edu

Author Contributions

The manuscript was written through contributions of all
authors. All authors have given approval to the final version
of the manuscript.

Notes

The authors declare no competing financial interest.

ACKNOWLEDGEMENTS

This work was supported by NSF CAREER (CHE-1654274), with co-funding from the Division of Molecular and Cellular Biosciences to FFL. We will like to acknowledge Dr. Mark E. Ridgeway and Dr. Mel A. Park support during the development and installation of the custom nESI-TIMS-MS instruments.

REFERENCES

1. H. Siegel and A. Siegel, *Biological Action of Metal Ions*, Marcel Dekker, New York, 1976.
2. C. M. Gomes and P. Wittung-Stafshede, *Protein Folding and Metal Ions: Mechanisms, Biology and Disease*, Taylor & Francis, Boca Raton, 2011.
3. E. A. Permyakov, *Metalloproteomics*, Wiley, New Jersey, 2009.
4. B. Zambelli, F. Musiani and S. Ciurli, *Met. Ions Life Sci.*, 2012, **10**, 135-170.
5. L. M. Teesch, R. C. Orlando and J. Adams, *J. Am. Chem. Soc.*, 1991, **113**, 3668-3675.
6. J. A. Loo, P. Hu and R. D. Smith, *J. Am. Soc. Mass Spectrom.*, 1994, **5**, 959-965.
7. O. V. Nemirovskiy and M. L. Gross, *J. Am. Soc. Mass Spectrom.*, 1998, **9**, 1020-1028.
8. P. F. Hu and J. A. Loo, *J. Am. Chem. Soc.*, 1995, **117**, 11314-11319.
9. P. B. Armentrout, M. T. Rodgers, J. Oomens and J. D. Steill, *J. Phys. Chem. A*, 2008, **112**, 2248-2257.
10. T. Wyttenbach, D. Liu and M. T. Bowers, *J. Am. Chem. Soc.*, 2008, **130**, 5993-6000.
11. R. H. Holm, P. Kennepohl and E. I. Solomon, *Chem. Rev.*, 1996, **96**, 2239-2314.
12. M. J. Page and E. Di Cera, *Physiol. Rev.*, 2006, **86**, 1049-1092.
13. C. Zentz, G. Chottard and J. Bolard, *J. Inorg. Nucl. Chem.*, 1978, **40**, 2019-2023.
14. L. Quintanar and L. Rivillas-Acevedo, *Methods Mol. Biol.*, 2013, **1008**, 267-297.
15. I. Bertini, P. Turano and A. J. Vila, *Chem. Rev.*, 1993, **93**, 2833-2932.
16. M. R. Jensen, M. A. Hass, D. F. Hansen and J. J. Led, *Cell. Mol. Life Sci.*, 2007, **64**, 1085-1104.
17. E. Ennifar, P. Walter and P. Dumas, *Nucleic Acids Res.*, 2003, **31**, 2671-2682.
18. S. E. J. Bowman, J. Bridwell-Rabb and C. L. Drennan, *Acc. Chem. Res.*, 2016, **49**, 695-702.
19. M. Kohtani, B. S. Kinnear and M. F. Jarrold, *J. Am. Chem. Soc.*, 2000, **122**, 12377-12378.
20. M. K. Drayss, P. B. Armentrout, J. Oomens and M. Schaefer, *Int. J. Mass Spectrom.*, 2010, **297**, 18-27.
21. J. Pan and L. Konermann, *Biochem.*, 2010, **49**, 3477-3486.
22. L. Deng, N. Sun, E. N. Kitova and J. S. Klassen, *Anal. Chem.*, 2010, **82**, 2170-2174.
23. J. T. Hopper and N. J. Oldham, *Anal. Chem.*, 2011, **83**, 7472-7479.
24. J. B. Fenn, M. Mann, C. K. Meng, S. F. Wong and C. M. Whitehouse, *Science*, 1989, **246**, 64-71.
25. L. M. Teesch and J. Adams, *J. Am. Chem. Soc.*, 1991, **113**, 812-820.
26. H. M. Watson, J. B. Vincent and C. J. Cassady, *J. Mass Spectrom.*, 2011, **46**, 1099-1107.
27. H. Liu and K. Hakansson, *Anal. Chem.*, 2006, **78**, 7570-7576.
28. A. J. Kleinnijenhuis, R. Mihalca, R. M. A. Heeren and A. J. R. Heck, *Int. J. Mass Spectrom.*, 2006, **253**, 217-224.
29. W. A. Tao, D. Zhang, E. N. Nikolaev and R. G. Cooks, *J. Am. Chem. Soc.*, 2000, **122**, 10598-10609.
30. J. Zhang and J. S. Brodbelt, *J. Mass Spectrom.*, 2003, **38**, 555-572.
31. J. Zhang and J. S. Brodbelt, *Anal. Chem.*, 2005, **77**, 1761-1770.
32. Y. Wu, C. Guo, N. Zhang, G. Bian and K. Jiang, *Rapid Commun. Mass Spectrom.*, 2014, **28**, 2111-2120.
33. L. Han and C. E. Costello, *J. Am. Soc. Mass Spectrom.*, 2011, **22**, 997-1013.
34. D. E. Clemmer, R. R. Hudgins and M. F. Jarrold, *J. Am. Chem. Soc.*, 1995, **117**, 10141-10142.
35. F. Lanucara, S. W. Holman, C. J. Gray and C. E. Eyers, *Nat. Chem.*, 2014, **6**, 281-294.
36. D. R. Fuller, M. S. Glover, N. A. Pierson, D. Kim, D. H. Russell and D. E. Clemmer, *J. Am. Soc. Mass Spectrom.*, 2016, **27**, 1376-1382.
37. C. Wu, J. Klasmeier and H. H. Hill, *Rapid Commun. Mass Spectrom.*, 1999, **13**, 1138-1142.
38. Y. Berezovskaya, C. T. Armstrong, A. L. Boyle, M. Porrini, D. N. Woolfson and P. E. Barran, *Chem. Commun.*, 2011, **47**, 412-414.
39. M. Kohtani, M. F. Jarrold, S. Wee and R. A. J. O'Hair, *J. Phys. Chem. B*, 2004, **108**, 6093-6097.
40. T. Wyttenbach, M. Witt and M. T. Bowers, *J. Am. Chem. Soc.*, 2000, **122**, 3458-3464.
41. Y. Seo, M. R. Schenauer and J. A. Leary, *Int. J. Mass Spectrom.*, 2011, **303**, 191-198.
42. V. E. Wright, F. Castro-Gómez, E. Jurneczko, J. C. Reynolds, A. Poulton, S. D. R. Christie, P. Barran, C. Bo and C. S. Creaser, *Int. J. Ion Mobil. Spectrom.*, 2013, **16**, 61-67.
43. J. M. Dilger, S. J. Valentine, M. S. Glover, M. A. Ewing and D. E. Clemmer, *Int. J. Mass Spectrom.*, 2012, **330**, 35-45.
44. T. G. Flick, I. D. Campuzano and M. D. Bartberger, *Anal. Chem.*, 2015, **87**, 3300-3307.
45. V. Domalain, V. Tognetti, M. Hubert-Roux, C. M. Lange, L. Joubert, J. Baudoux, J. Rouden and C. Afonso, *J. Am. Soc. Mass Spectrom.*, 2013, **24**, 1437-1445.
46. B. H. Clowers and H. H. Hill, Jr., *J. Mass Spectrom.*, 2006, **41**, 339-351.
47. M. D. Leavell, S. P. Gaucher, J. A. Leary, J. A. Taraszka and D. E. Clemmer, *J. Am. Soc. Mass Spectrom.*, 2002, **13**, 284-293.
48. F. A. Fernandez-Lima, D. A. Kaplan, J. Suetering and M. A. Park, *Int. J. Ion Mobil. Spectrom.*, 2011, **14**, 93-98.
49. F. A. Fernandez-Lima, D. A. Kaplan and M. A. Park, *Rev. Sci. Instr.*, 2011, **82**, 126106.
50. D. R. Hernandez, J. D. Debord, M. E. Ridgeway, D. A. Kaplan, M. A. Park and F. Fernandez-Lima, *Analyst*, 2014, **139**, 1913-1921.
51. P. Benigni, C. J. Thompson, M. E. Ridgeway, M. A. Park and F. Fernandez-Lima, *Anal. Chem.*, 2015, **87**, 4321-4325.

52. P. Benigni and F. Fernandez-Lima, *Anal. Chem.*, 2016, **88**, 7404-7412.
53. P. Benigni, K. Sandoval, C. J. Thompson, M. E. Ridgeway, M. A. Park, P. Gardinali and F. Fernandez-Lima, *Environ. Sci. Technol.*, 2017, **51**, 5978-5988.
54. K. J. Adams, D. Montero, D. Aga and F. Fernandez-Lima, *Int. J. Ion Mobil. Spectrom.*, 2016, **19**, 69-76.
55. A. Castellanos, P. Benigni, D. R. Hernandez, J. D. DeBord, M. E. Ridgeway, M. A. Park and F. A. Fernandez-Lima, *Anal. Meth.*, 2014, **6**, 9328-9332.
56. E. R. Schenk, V. Mendez, J. T. Landrum, M. E. Ridgeway, M. A. Park and F. Fernandez-Lima, *Anal. Chem.*, 2014, **86**, 2019-2024.
57. J. C. Molano-Arevalo, D. R. Hernandez, W. G. Gonzalez, J. Miksovskaa, M. E. Ridgeway, M. A. Park and F. Fernandez-Lima, *Anal. Chem.*, 2014, **86**, 10223-10230.
58. A. McKenzie-Coe, J. D. DeBord, M. Ridgeway, M. Park, G. Eiceman and F. Fernandez-Lima, *Analyst*, 2015, **140**, 5692-5699.
59. A. Garabedian, D. Butcher, J. L. Lippens, J. Miksovskaa, P. P. Chapagain, D. Fabris, M. E. Ridgeway, M. A. Park and F. Fernandez-Lima, *Phys. Chem. Chem. Phys.*, 2016, **18**, 26691-26702.
60. M. E. Ridgeway, J. A. Silveira, J. E. Meier and M. A. Park, *Analyst*, 2015, **140**, 6964-6972.
61. F. Meier, S. Beck, N. Grassl, M. Lubeck, M. A. Park, O. Raether and M. Mann, *J. Proteome Res.*, 2015, **14**, 5378-5387.
62. J. A. Silveira, M. E. Ridgeway and M. A. Park, *Anal. Chem.*, 2014, **86**, 5624-5627.
63. Y. Pu, M. E. Ridgeway, R. S. Glaskin, M. A. Park, C. E. Costello and C. Lin, *Anal. Chem.*, 2016, **88**, 3440-3443.
64. F. C. Liu, S. R. Kirk and C. Bleiholder, *Analyst*, 2016, **141**, 3722-3730.
65. A. Garabedian, P. Benigni, C. E. Ramirez, E. S. Baker, T. Liu, R. D. Smith and F. Fernandez-Lima, *J. Am. Soc. Mass Spectrom.*, 2017, DOI: 10.1007/s13361-017-1787-8.
66. E. R. Schenk, M. E. Ridgeway, M. A. Park, F. Leng and F. Fernandez-Lima, *Anal. Chem.*, 2014, **86**, 1210-1214.
67. K. Jeanne Dit Fouque, A. Garabedian, J. Porter, M. Baird, X. Pang, T. D. Williams, L. Li, A. Shvartsburg and F. Fernandez-Lima, *Anal. Chem.*, 2017, **89**, 11787-11794.
68. E. R. Schenk, R. Almeida, J. Miksovskaa, M. E. Ridgeway, M. A. Park and F. Fernandez-Lima, *J. Am. Soc. Mass Spectrom.*, 2015, **26**, 555-563.
69. J. C. Molano-Arevalo, K. Jeanne Dit Fouque, K. Pham, J. Miksovskaa, M. E. Ridgeway, M. A. Park and F. Fernandez-Lima, *Anal. Chem.*, 2017, **89**, 8757-8765.
70. P. Benigni, R. Marin, J. C. Molano-Arevalo, A. Garabedian, J. J. Wolff, M. E. Ridgeway, M. A. Park and F. Fernandez-Lima, *Int. J. Ion Mobil. Spectrom.*, 2016, **19**, 95-104.
71. J. D. Hegemann, M. Zimmermann, X. Xie and M. A. Marahiel, *Acc. Chem. Res.*, 2015, **48**, 1909-1919.
72. M. O. Maksimov, S. J. Pan and A. James Link, *Nat. Prod. Rep.*, 2012, **29**, 996-1006.
73. J. D. Hegemann, M. Zimmermann, S. Zhu, D. Klug and M. A. Marahiel, *Biopolymers*, 2013, **100**, 527-542.
74. J. D. Hegemann, M. Zimmermann, X. Xie and M. A. Marahiel, *J. Am. Chem. Soc.*, 2013, **135**, 210-222.
75. M. O. Maksimov and A. J. Link, *J. Ind. Microbiol. Biotechnol.*, 2014, **41**, 333-344.
76. M. O. Maksimov, I. Pelczer and A. J. Link, *Proc. Natl. Acad. Sci. USA*, 2012, **109**, 15223-15228.
77. R. D. Kersten, Y. L. Yang, Y. Xu, P. Cimermancic, S. J. Nam, W. Fenical, M. A. Fischbach, B. S. Moore and P. C. Dorrestein, *Nat. Chem. Biol.*, 2011, **7**, 794-802.
78. J. I. Tietz, C. J. Schwalen, P. S. Patel, T. Maxson, P. M. Blair, H. C. Tai, U. I. Zakai and D. A. Mitchell, *Nat. Chem. Biol.*, 2017, **13**, 470-478.
79. T. A. Knappe, F. Manzenrieder, C. Mas-Moruno, U. Linne, F. Sasse, H. Kessler, X. Xie and M. A. Marahiel, *Angew. Chem. Int. Ed. Engl.*, 2011, **50**, 8714-8717.
80. J. D. Hegemann, M. De Simone, M. Zimmermann, T. A. Knappe, X. Xie, F. S. Di Leva, L. Marinelli, E. Novellino, S. Zahler, H. Kessler and M. A. Marahiel, *J. Med. Chem.*, 2014, **57**, 5829-5834.
81. J. D. Hegemann, C. D. Fage, S. Zhu, K. Harms, F. S. Di Leva, E. Novellino, L. Marinelli and M. A. Marahiel, *Mol. Biosyst.*, 2016, **12**, 1106-1109.
82. M. Zimmermann, J. D. Hegemann, X. Xie and M. A. Marahiel, *Chem. Biol.*, 2013, **20**, 558-569.
83. T. A. Knappe, U. Linne, L. Robbel and M. A. Marahiel, *Chem. Biol.*, 2009, **16**, 1290-1298.
84. R. A. Salomon and R. N. Farias, *J. Bacteriol.*, 1992, **174**, 7428-7435.
85. J. O. Solbiati, M. Ciaccio, R. N. Farias, J. E. Gonzalez-Pastor, F. Moreno and R. A. Salomon, *J. Bacteriol.*, 1999, **181**, 2659-2662.
86. E. W. McDaniel and E. A. Mason, *Mobility and diffusion of ions in gases*, John Wiley and Sons, Inc., New York, New York, 1973.
87. K. Jeanne Dit Fouque, J. Moreno, J. D. Hegemann, S. Zirah, S. Rebuffat and F. Fernandez-Lima, *Anal. Chem.*, 2018.
88. K. Jeanne Dit Fouque, H. Lavanant, S. Zirah, J. Lemoine, S. Rebuffat, J. C. Tabet, A. Kulesza, C. Afonso, P. Dugourd and F. Chiro, *Rapid Commun. Mass Spectrom.*, 2015, **29**, 1411-1419.
89. K. Jeanne Dit Fouque, H. Lavanant, S. Zirah, V. Steinmetz, S. Rebuffat, P. Maitre and C. Afonso, *J. Phys. Chem. A*, 2016, **120**, 3810-3816.
90. K. J. Rosengren, R. J. Clark, N. L. Daly, U. Goeransson, A. Jones and D. J. Craik, *J. Am. Chem. Soc.*, 2003, **125**, 12464-12474.
91. J. A. Taraszka, A. E. Counterman and D. E. Clemmer, *Int. J. Mass Spectrom.*, 2001, **204**, 87-100.
92. M. O. Maksimov and A. J. Link, *J. Am. Chem. Soc.*, 2013, **135**, 12038-12047.
93. J. R. Chekan, J. D. Koos, C. Zong, M. O. Maksimov, A. J. Link and S. K. Nair, *J. Am. Chem. Soc.*, 2016, **138**, 16452-16458.
94. K. Jeanne Dit Fouque, C. Afonso, S. Zirah, J. D. Hegemann, M. Zimmermann, M. A. Marahiel, S. Rebuffat and H. Lavanant, *Anal. Chem.*, 2015, **87**, 1166-1172.